N-Donor Competition in Iron Bis(chelate) Bis(pyrazolyl)pyridinylmethane Complexes

Ulrich Herber[a], Alexander Hoffmann[a], Charles Lochenie[b], Birgit Weber[b], and Sonja Herres-Pawlis[a]

[a] Department Chemie, Ludwig-Maximilians-Universität München, Butenandtstr. 5 – 13, 81377 München, Germany

[b] Universität Bayreuth, Anorganische Chemie II, Universitätsstraße 30, NW I, 95440 Bayreuth, Germany

Reprint requests to Prof. Dr. S. Herres-Pawlis. Fax: 089-218077904.
E-mail: sonja.herres-pawlis@cup.uni-muenchen.de

Z. Naturforsch. **2014**, *69b*, 1206 – 1214 / DOI: 10.5560/ZNB.2014-4176
Received August 5, 2014

Dedicated to Professor Hubert Schmidbaur on the occasion of his 80th birthday

We report on the synthesis and structural characterisation of the bis(chelate) bis(pyrazolyl)pyridinylmethane iron(II) complexes $[Fe\{HC(Pz)_2(Py)\}_2][CF_3CO_2]_2$, $[Fe\{HC(3\text{-}iPrPz)(5\text{-}iPrPz)(Py)\}_2][CF_3SO_3]_2$ and $[Fe\{HC(3\text{-}iPrPz)(5\text{-}iPrPz)(Py)\}_2][FeBr_4]Br{\cdot}2C_4H_8O$. During the synthesis of the latter ones, an isomerisation of the ligand is observed: the pyrazolyl substituent formally moves from the 3 to the 5 position. Since the donor competition between pyrazolyl and pyridinyl moieties is important for the coordination properties, we also studied the donor properties by density functional theory and natural bond orbital analysis (NBO). As a result, the pyridinyl donor is generally weaker than the pyrazolyl donor, but the pyrazolyl donor is heavily influenced by the alkyl substitution pattern. To confirm the low-spin state of the complexes, magnetic susceptibility measurements have been performed.

Key words: Iron, Bis(pyrazolyl)methane Complexes, X-Ray Crystallography, DFT, NBO

Introduction

Bis(pyrazolyl)methane ligands have emerged in coordination chemistry and especially in bioinorganic chemistry during the last years [1 – 8]. They offer a facial tridentate coordination environment for a multitude of metals [1 – 8]. Especially their combination with pyridinyl as a third donor function has been shown to be promising for the synthesis of tyrosinase models [9, 10]. Here, a donor competition between the pyridinyl and the pyrazolyl units can be observed. Regarding basicity, pyridine is three pK_a units more basic than pyrazole [11]. The relative donor strengths can be tuned through suited substitution as a subtle interplay of basicity and nucleophilicity [12, 13]. The pyrazolyl/pyridinyl donor competition is normally won by pyrazolyl, but small distortions of the metal's coordinative preferences such as the Jahn–Teller distortion can change the picture [14].

Herein, we report on bis(chelate) iron complexes coordinated by bis(pyrazolyl)methane ligands. Besides the unsubstituted ligand (2-pyridinyl)bis(pyrazolyl)methane ($HC(Pz)_2(Py)$) which was originally reported by Canty *et al.* [15], we investigated the pyrazolyl-substituted ligand (2-pyridinyl)bis(3-*iso*-propylpyrazolyl)methane $HC(3\text{-}iPrPz)_2(Py)$ [16]. The substitution at the 3-position shall prevents the formation of bis(chelate) complexes and opens up coordination sites for catalytic reactivity. Remarkably, the systems sometimes try to avoid the steric pressure, and rearrangements of the substituents from 3- to 5-position occur when Lewis acids are present [17, 18]. This 3- to 5-isomerisation also happens when $HC(3\text{-}iPrPz)_2(Py)$ reacts with iron(II) and again, bis(chelate) complexes are obtained. We investigated the donor competition

within these complexes by natural bond orbital analysis. Bis(chelate) iron complexes with *N*-donor ligands have found great attention in the field of spin crossover applications [19 – 23]. Small changes in substituents can influence the ligand field in such a way that the spin transition is facilitated at higher temperatures.

Results and Discussion

Synthesis and molecular structures of (2-pyridinyl)bis(pyrazolyl)methane iron complexes

Fe(II) tends to form octahedral bisfacial complexes with (2-pyridinyl)bis(pyrazolyl)methane ligands [14]. Thus the reaction of $Fe(CF_3CO_2)_2$ and (2-pyridinyl)bis(pyrazolyl)methane ($HC(Pz)_2(Py)$) leads to the bis(chelate) complex $[Fe\{HC(Pz)_2(Py)\}_2][CF_3CO_2]_2$ (**1[CF$_3$CO$_2$]$_2$**) (Scheme 1), while the complexes $[Fe\{HC(3\text{-}i\text{PrPz})(5\text{-}i\text{PrPz})(Py)\}_2][CF_3SO_3]_2$ (**2[CF$_3$SO$_3$]$_2$**) and $[Fe\{HC(3\text{-}i\text{PrPz})(5\text{-}i\text{PrPz})(Py)\}_2][FeBr_4]Br\cdot 2C_4H_8O$ (**2[FeBr$_4$]Br**) are obtained by reacting (2-pyridinyl)bis(3-*iso*-propylpyrazolyl)methane $HC(3\text{-}i\text{PrPz})_2(Py)$ with $Fe(CF_3CO_2)_2$ and $FeBr_2$, respectively (Scheme 2). During complex formation one *iso*-propylpyrazolyl unit undergoes isomerisation resulting in HC(3-*i*PrPz)(5-*i*PrPz)(Py) as the coordinating ligand. In all three complexes, the pyridinyl

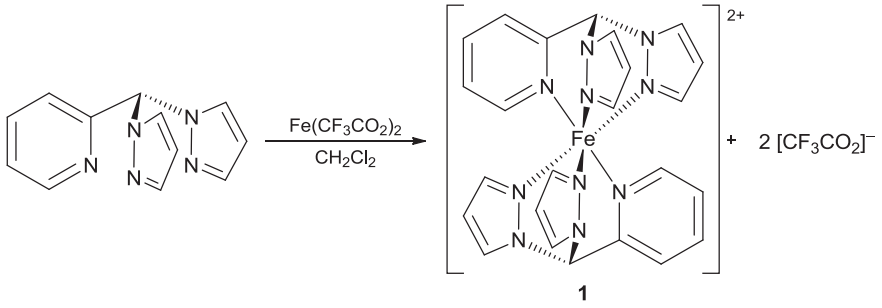

Scheme 1. Synthesis of $[Fe\{HC(Pz)_2(Py)\}_2][CF_3CO_2]_2$ (**1[CF$_3$CO$_2$]$_2$**).

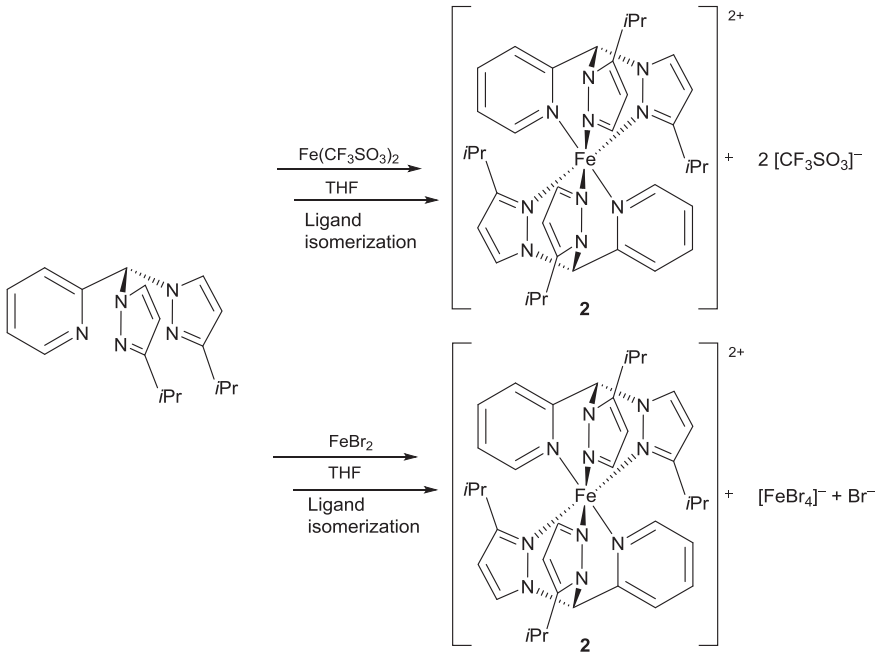

Scheme 2. Synthesis of $[Fe\{HC(3\text{-}i\text{PrPz})(5\text{-}i\text{PrPz})(Py)\}_2][CF_3SO_3]_2$ (**2[CF$_3$SO$_3$]$_2$**) and $[Fe\{HC(3\text{-}i\text{PrPz})(5\text{-}i\text{PrPz})(Py)\}_2][FeBr_4]Br\cdot 2C_4H_8O$ (**2[FeBr$_4$]Br**).

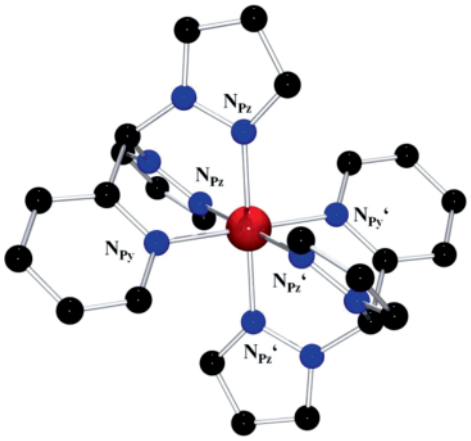

Fig. 1 (colour online). Molecular structure of the cationic complex $[Fe\{HC(Pz)_2(Py)\}_2]^{2+}$ (**1**) in crystals of **1[CF$_3$CO$_2$]$_2$**.

moieties are *trans*-positioned as also found in related complexes [14].

The octahedral coordination of the central metal by two ligands is supported by HR-ESI-MS, showing the according mass peaks for the cationic complexes together with one corresponding counter ion. The molecular structures of all three complexes were determined by single-crystal X-ray diffraction. $[Fe\{HC(Pz)_2(Py)\}_2][CF_3CO_2]_2$ (**1[CF$_3$CO$_2$]$_2$**) crystallises in the triclinic crystal system, space group $P\bar{1}$ ($Z = 1$), as a symmetrical octahedral cationic complex with two counter ions in the outer coordination sphere (Fig. 1) and the iron(II) ion residing on a crystallographic centre of inversion.

The N–Fe–N angles varying from 87.4(1) to 88.9(1)° show that the octahedron is only slightly distorted. Both Fe–N_{pz} distances are almost equal with 1.971(2) and 1.969(2) Å, but shorter than the Fe–N_{py} distance with 1.991(2) Å (Table 1).

The complexes $[Fe\{HC(3\text{-}iPrPz)(5\text{-}iPrPz)(Py)\}_2][CF_3SO_3]_2$ (**2[CF$_3$SO$_3$]$_2$**) and $[Fe\{HC(3\text{-}iPrPz)(5\text{-}iPrPz)(Py)\}_2][FeBr_4]Br{\cdot}2C_4H_8O$ (**2[FeBr$_4$]Br**) crystallise in the same space group as **1[CF$_3$CO$_2$]$_2$**. Selected bond lengths and angles are summarised in Table 1. Crystallographic details are given in Table 2. During complex formation one *i*PrPz moiety undergoes isomerisation from the 3- to the 5-position (Fig. 2). As a result, the pyrazolyl units differ with regard to their Fe–N bond lengths. The Fe–$N_{5\text{-}iPrPz}$ bonds (1.957(3) Å for **2[CF$_3$SO$_3$]$_2$** and 1.957(5) Å for **2[FeBr$_4$]Br**) are shorter than the Fe–$N_{3\text{-}iPrPz}$ bonds (1.991(3) Å for **2[CF$_3$SO$_3$]$_2$** and 1.998(5) Å for **2[FeBr$_4$]Br**).

Table 1. Selected bond lengths (Å) and angles (deg) for $[Fe\{HC(Pz)_2(Py)\}_2][CF_3CO_2]_2$ (**1[CF$_3$CO$_2$]$_2$**), $[Fe\{HC(3\text{-}iPrPz)(5\text{-}iPrPz)(Py)\}_2][CF_3SO_3]_2$ (**2[CF$_3$SO$_3$]$_2$**) and $[Fe\{HC(3\text{-}iPrPz)(5\text{-}iPrPz)(py)\}_2][FeBr_4]Br \cdot 2C_4H_8O$ (**2[FeBr$_4$]Br**).

	1[CF$_3$CO$_2$]$_2$	**2[CF$_3$SO$_3$]$_2$**	**2[FeBr$_4$]Br**
Bond lengths			
Fe–N_{Py}	1.991(2)	1.994(3)	1.981(5)
Fe–$N_{5\text{-}iPrPz}$	1.969(2)[a]	1.957(3)	1.957(5)
Fe–$N_{3\text{-}iPrPz}$	1.971(2)[a]	1.991(3)	1.998(5)
Bond angles			
N_{Py}–Fe–$N_{5\text{-}iPrPz}$	87.4(1)[a]	89.2(1)	89.2(2)
N_{Py}–Fe–$N_{3\text{-}iPrPz}$	87.5(1)[a]	87.3(1)	87.7(2)
$N_{3\text{-}iPrPz}$–Fe–$N_{5\text{-}iPrPz}$	88.9(1)[a]	88.2(1)	88.1(2)

[a] **1**: 5-*i*PrPz and 3-*i*PrPz are Pz.

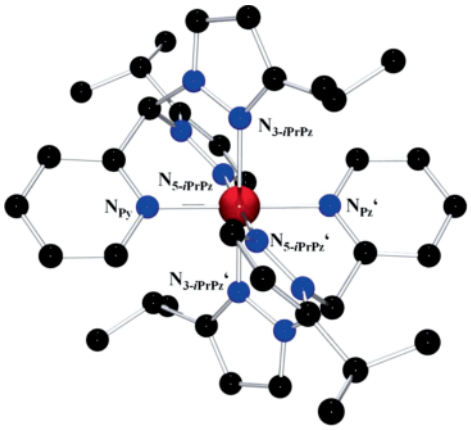

Fig. 2 (colour online). Molecular structure of $[Fe\{HC(3\text{-}iPrPz)(5\text{-}iPrPz)(Py)\}_2]^{2+}$ (**2**) in crystals of **2[CF$_3$SO$_3$]$_2$** and **2[FeBr$_4$]Br**.

DFT calculations and NBO analyses

In addition to the experiments, theoretical calculations were conducted, starting with a small structural benchmarking to determine a method that describes the experimental results correctly. At first complex **1[CF$_3$CO$_2$]$_2$** was determined to be a low-spin complex by a SQUID measurement with a room temperature $\chi_M T$ product of 0.61 cm^3 K mol^{-1}. In Fig. 3 the temperature dependence is given, proving that the spin state does not change significantly in the whole investigated temperature range (10 – 400 K).

Table 2. Crystal structure data for **1[CF_3CO_2]$_2$**, **2[CF_3SO_3]$_2$** and **2[$FeBr_4$]Br**.

	1[CF_3CO_2]$_2$	**2[CF_3SO_3]$_2$**	**2[$FeBr_4$]Br · 2C_4H_8O**
Empirical formula	$C_{28}H_{22}F_6FeN_{10}O_4$	$C_{38}H_{46}F_6FeN_{10}O_6S_2$	$C_{44}H_{62}Br_5Fe_2N_{10}O_2$
M_r	732.41	972.82	1274.29
Crystal size, mm^3	0.16 × 0.12 × 0.10	0.08 × 0.05 × 0.03	0.11 × 0.05 × 0.04
Crystal system	triclinic	triclinic	triclinic
Space group	$P\bar{1}$	$P\bar{1}$	$P\bar{1}$
a, Å	7.6068(3)	9.203(3)	11.9105(8)
b, Å	10.8017(4)	9.730(3)	12.8265(10)
c, Å	11.4394(4)	12.709(4)	17.0875(13)
α, deg	113.225(1)	97.818(8)	89.996(2)
β, deg	101.845(1)	98.472(9)	87.385(2)
γ, deg	102.853(1)	92.520(9)	86.834(2)
V, Å^3	795.82(5)	1112.8(6)	2603.8(3)
Z	1	1	2
$D_{calcd.}$, g cm^{-3}	1.53	1.45	1.63
μ(Mo K$_\alpha$), mm^{-1}	0.6	0.5	4.4
F(000), e	372	504	1278
hkl range	±9, ±14, ±14	±10, ±11, ±15	−14/+13, ±15, ±20
θ_{max}, deg	27.51	25.02	25.02
Refl. collected	16 130	8415	45 068
Refl. unique	3605	3891	9162
R_{int}	0.0268	0.0874	0.0939
No. parameters	223	318	579
$R(F)$[a] [$I > 2\,\sigma(I)$]	0.0479	0.0540	0.0535
$wR(F^2)$[b] (all data)	0.1244	0.1325	0.1412
GoF (F^2)[c]	1.062	0.956	1.022
$\Delta\rho_{fin}$ (max/min), e Å^{-3}	1.15/−0.69	0.48/−0.43	1.39/−1.08

[a] $R(F) = \Sigma||F_o| - |F_c||/\Sigma|F_o|$; [b] $wR(F^2) = [\Sigma w(F_o^2 - F_c^2)^2/\Sigma w(F_o^2)^2]^{1/2}$, $w = [\sigma^2(F_o^2) + (AP)^2 + BP]^{-1}$, where $P = (\mathrm{Max}(F_o^2, 0) + 2F_c^2)/3$; [c] GoF $= [\Sigma w(F_o^2 - F_c^2)^2/(n_{obs} - n_{param})]^{1/2}$.

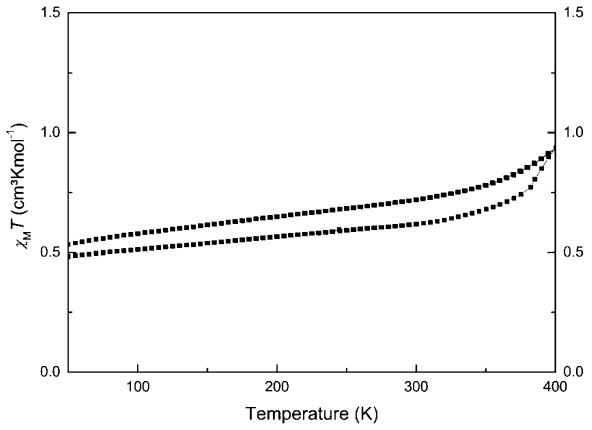

Fig. 3. Plot of the $\chi_M T$ product *versus* T for **1[CF_3CO_2]$_2$**.

Table 3. Selected experimental and calculated bond lengths (Å) and angles (deg) for [Fe{HC(Pz)$_2$(Py)}$_2$][CF_3CO_2]$_2$ (**1[CF_3CO_2]$_2$**).

	1	BP86/ 6-31 +g(d)	BP86/ 6-311 +g(d)	B3LYP/ 6-31 +g(d)	B3LYP/ 6-311 +g(d)
Bond lengths					
Fe–N_{Py}	1.991(2)	1.981	1.985	2.033	2.041
Fe–N_{Pz}	1.969(2)	1.959	1.965	2.005	2.014
	1.971(2)	1.959	1.966	2.005	2.014
Bond angles					
N_{Py}–Fe–N_{Pz}	87.4(1)	88.0	87.9	87.1	87.0
	87.5(1)	88.0	87.9	87.1	87.0
N_{Pz}–Fe–N_{Pz}	88.9(1)	89.1	89.0	88.2	88.1

The selected functionals are B3LYP and BP86 in combination with the Pople basis sets 6-31+g(d) and 6-311+g(d). The results show a greater accordance of structural data between theory and experiment for the BP86 functional than for B3LYP (Table 3). Furthermore the use of the triple-zeta basis 6-311+g(d) gives more accurate results than 6-31+g(d), where all bond lengths are too short. With regard to the calculated angles BP86 and B3LYP are showing good accordance with the results of the crystal structure. A variation of the basis set has almost no impact on the calculated angles.

As a result of this study, BP86/6-311+g(d) was applied in NBO3 and NBO6 second order perturba-

Table 4. Calculated NBO interaction energies E (kcal mol^{-1}) for $[Fe\{HC(Pz)_2(Py)\}_2]^{2+}$ (**1**) and for $[Fe\{HC(3\text{-}i\text{PrPz})(5\text{-}i\text{PrPz})(Py)\}_2]^{2+}$ (**2**) (BP86/6-311+g(d)).

1	E (NBO3)	E (NBO6)	**2**	E (NBO3)	E (NBO6)
$N_{Py} \rightarrow Fe$	179	133	$N_{Py} \rightarrow Fe$	162	129
$N_{Pz} \rightarrow Fe$	198	141	$N_{5\text{-}i\text{PrPz}} \rightarrow Fe$	181	137
	198	141	$N_{3\text{-}i\text{PrPz}} \rightarrow Fe$	163	124

tion theory analysis of the cation **1** to get an insight into the donor abilities of the different coordination functionalities with regard to the NBO version. By donating electron density from the nitrogen lone-pair to the metal centre both pyrazolyl units provide a stabilising energy of 198/141 kcal mol^{-1} (NBO3/NBO6), while the pyridinyl moiety supplies only 179/131 kcal mol^{-1} and hence is the weaker donor (Table 4). These energies show a correlation between the donor ability and the bond length within this complex, and they show a significant decrease from NBO3 to NBO6. These results are in accordance with the results obtained for the same cation with a smaller basis set [14].

Regarding **2**, the prior benchmarking with the same functionals and basis sets also results in BP86/6-311+g(d) as the most appropriate method. With respect to the similarity of the cationic complexes of **2** in the crystals of **2[CF$_3$SO$_3$]$_2$** and **2[FeBr$_4$]Br** both were considered to be equal for all calculations. The NBO analysis confirms the inequality of the differently substituted pyrazolyl isomers. The pyridinyl unit is again the weakest donor with 162 kcal mol^{-1}, and 5-*i*PrPz is the strongest with 181 kcal mol^{-1}. In NBO6 calculations, 3-*i*PrPz is the weakest donor with 124 kcal mol^{-1}. Irrespective of the NBO version 3-*i*PrPz is significantly weaker as donor functionality with 163/124 (NBO3/NBO6) kcal mol^{-1} than 5-*i*PrPz, correlating again with the Fe–N bond lengths.

Based on the experimentally observed isomerisation processes during complex formation DFT calculations were performed on the different isomers. Using BP86/6-311+g(d) structural optimisations were performed for the experimentally obtained complex cation $[Fe\{HC(3\text{-}i\text{PrPz})(5\text{-}i\text{PrPz})(Py)\}_2]^{2+}$ (**2**) (Fig. 2), as well as for the model complex $[Fe\{HC(3\text{-}i\text{PrPz})_2(Py)\}_2]^{2+}$ (**3**) (Fig. 4) giving an energy difference of 20 kcal mol^{-1} in favour of the 3,5-isomer. This energy difference seems to drive the isomerisation as has also been calculated in other cases [18].

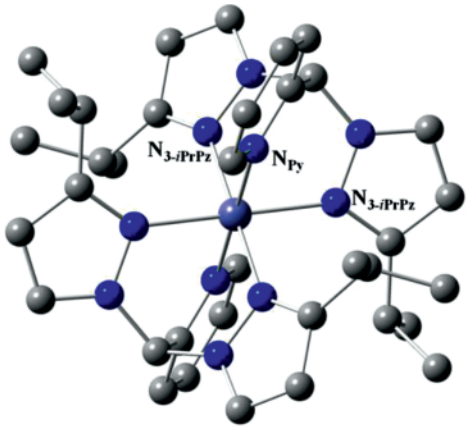

Fig. 4 (colour online). Molecular structure of the model complex $[Fe\{HC(3\text{-}i\text{PrPz})_2(Py)\}_2]^{2+}$ (**3**). Fe–N_{Py} 1.986 Å, Fe–$N_{3\text{-}i\text{PrPz}}$ 2.020 Å.

Table 5. Calculated NBO interaction energies E (kcal mol^{-1}) for $[Fe\{HC(3\text{-}i\text{PrPz})_2(Py)\}_2]^{2+}$ (**3**) (BP86/6-311+g(d)).

	E (NBO3)	E (NBO6)
$N_{Py} \rightarrow Fe$	141	119
$N_{3\text{-}i\text{PrPz}} \rightarrow Fe$	150; 150	122

Further NBO analysis of the model complex **3** (Table 5) reveals a dependence of the pyrazolyl donor ability on the position of functionalisation. If no isomerisation takes place, both pyrazolyl donors provide the same amount of energy with 150/122 kcal mol^{-1} (NBO3/NBO6) and are stronger donors than the pyridinyl unit with 141/119 kcal mol^{-1} (NBO3/NBO6). Because of sterical hindrance the Fe–N bond lengths are larger in complex **3** than in **2**, due to the repulsion of the *iso*-propyl groups, leading to lower energies.

Hence, the donor ability is dependent on the position of the *iso*-propyl group, raising the question of the impact of different alkyl groups on the donor ability. Therefore, the methyl (**4**) and *tert*-butyl (**5**) derivates of **2** were built up by replacing the *iso*-propyl groups by the respective alkyls (Fig. 5).

At first, both complex structures were optimised, using BP86/6-311+g(d), and subsequently analysed by NBO second order perturbation theory (Table 6). A comparison of the Fe–N bond lengths reveals a continuous decrease in case of N_{Py} and $N_{5\text{-}Pz}$ from methyl to *tert*-butyl, while the Fe–$N_{3\text{-}Pz}$ distance increases (Table 6).

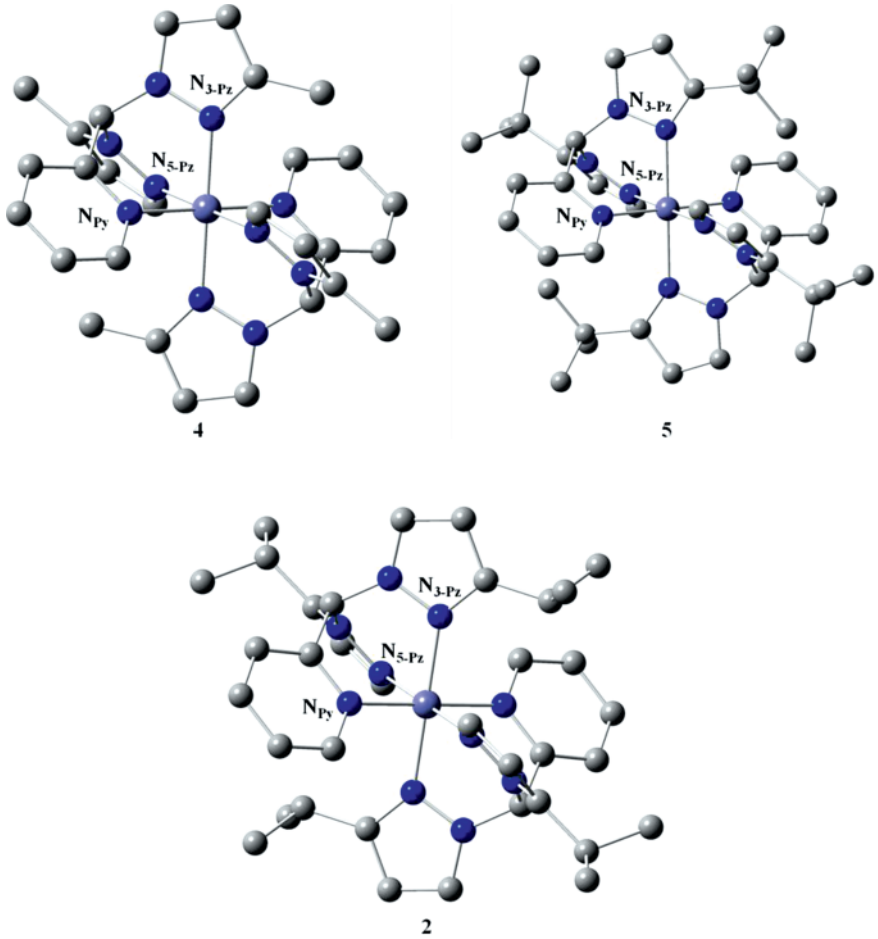

Fig. 5 (colour online). Calculated molecular structures of $[Fe\{HC(3\text{-}MePz)(5\text{-}MePz)(Py)\}_2]^{2+}$ (**4**), $[Fe\{HC(3\text{-}i\text{PrPz})(5\text{-}i\text{PrPz})(Py)\}_2]^{2+}$ (**2**) and $[Fe\{HC(3\text{-}t\text{BuPz})(5\text{-}t\text{BuPz})(Py)\}_2]^{2+}$ (**5**).

Table 6. Calculated Fe–N bond lengths (Å) for **4**, **2** and **5** (BP86/6-311+g(d)) with the respective alkyl rests in parentheses.

	4 (methyl)	**2** (*iso*-propyl)	**5** (*tert*-butyl)
Fe–N_{Py}	1.983	1.980	1.971
Fe–$N_{5\text{-}Pz}$	2.000	1.965	1.953
Fe–$N_{3\text{-}Pz}$	1.963	2.022	2.110

As shown in Table 7, there is an inverse correlation between bond length and donor ability (NBO3). Beside the decreasing Fe–N bond lengths for N_{Py} and $N_{5\text{-}Pz}$ the stabilising energies diminish as well with 17 kcal mol^{-1} for N_{Py} and 21 kcal mol^{-1} for $N_{5\text{-}Pz}$. In the case of $N_{3\text{-}Pz}$ an expected correlation of increasing bond length and decreasing stabilising interactions is obtained. The difference of 49 kcal mol^{-1} between **4** and **5** shows the strong influence of alkyl derivatisation on the donor ability of 3-functionalised pyrazolyl units. Another result is the correlation between the increasing difference of Fe–$N_{5\text{-}Pz}$ and Fe–$N_{3\text{-}Pz}$ bond lengths from 0.037 (**5**) to 0.157 Å and the increase of the corresponding energy differences from 13 to 41 kcal mol^{-1}. By contrast, for NBO6 all pyridinyl units are of equal donor strength with 129 kcal mol^{-1}, and the decrease for $N_{5\text{-}Pz}$ and $N_{3\text{-}Pz}$ is still given but not as significant as for NBO3.

The prior optimisation of the molecular structures of **4** and **5** leads to a misleading conclusion concerning the substituent effects because of changes in the molecular structure due to substituent repulsion. Thus,

Table 7. Calculated NBO interaction energies E (kcal mol^{-1}) for $[Fe\{HC(3\text{-}MePz)(5\text{-}MePz)(Py)\}_2]^{2+}$ (**4**), $[Fe\{HC(3\text{-}i PrPz)(5\text{-}i PrPz)(Py)\}_2]^{2+}$ (**2**) and $[Fe\{HC(3\text{-}t BuPz)(5\text{-}t BuPz)(Py)\}_2]^{2+}$ (**5**) (BP86/6-311+g(d)).

	4 (NBO3)	**4** (NBO6)	**2** (NBO3)	**2** (NBO6)	**5** (NBO3)	**5** (NBO6)
$N_{Py} \rightarrow Fe$	167	129	162	129	150	129
$N_{5\text{-}Pz} \rightarrow Fe$	188	139	181	137	167	135
$N_{3\text{-}Pz} \rightarrow Fe$	175	132	163	124	126	98

Table 8. Calculated NBO interaction energies E (kcal mol^{-1}) for (**4**), (**2**) and (**5**) with fixed coordinates to the values of cation **2** for all coordinating N atoms and the Fe atom (BP86/6-311+g(d)).

	4 (NBO3)	**4** (NBO6)	**2** (NBO3)	**2** (NBO6)	**5** (NBO3)	**5** (NBO6)
$N_{Py} \rightarrow Fe$	166	129	162	129	155	130
$N_{5\text{-}Pz} \rightarrow Fe$	185	137	180	137	171	135
$N_{3\text{-}Pz} \rightarrow Fe$	167	125	162	124	150	122

in a second approach the positions of the central metal and all coordinating nitrogen atoms were fixed to the values of cation **2**. Optimisation of the structures of **4** and **5** followed by NBO analysis leads to a different picture of the influences of derivatisation on the metal-ligand interactions. In these complexes 5-*i*PrPz is always the strongest donor. For the methyl compound (**4**) the stabilising energy decreases for all three donor functionalities by 1 kcal mol^{-1} for N_{Py}, 3 kcal mol^{-1} for $N_{5\text{-}Pz}$ and 8 kcal mol^{-1} for $N_{3\text{-}Pz}$ in comparison to the unconstrained complex (NBO3). By contrast, for compound **5** all stabilising energies increase by 5 kcal mol^{-1} for N_{Py}, 4 kcal mol^{-1} for $N_{5\text{-}Pz}$ and 25 kcal mol^{-1} for $N_{3\text{-}Pz}$ (Table 8) toward the non-restricted complex (NBO3). These changes in Fe–N bond lengths diminish the influence of derivatisation on the donor ability as well as the differences between $N_{5\text{-}Pz}$ and $N_{3\text{-}Pz}$. The results with NBO6 also show a decrease in energy compared to the unconstrained complex, although a smaller one, for all three donor functionalities for **4** and **5**. Overall, the $N_{5\text{-}Py}$ remains the strongest donor in all three complexes, whereas the $N_{3\text{-}Pz}$ appears to be weaker than the N_{Py} donor. The NBO6 calculations demonstrate that there is indeed a small influence of the derivatisation on the donor abilities.

Conclusion

The structural characterisation of bis(chelate) iron bis(pyrazolyl)pyridinylmethane complexes has shown that second generation ligands are able to stabilise a bis(chelate) coordination after ligand rearrangement in form of a 3→5 isomerisation of the pyrazolyl substituent. The experimental results were complemented by DFT studies which reveal that in the unsubstituted complex cation **1**, the donor ability of the pyrazolyl units is larger compared to that of the pyridinyl donors, but that the position of the substituents has a strong effect on the donor stabilisation energy. This is disclosed in the cation **2** as well as in the model cations **3**–**5** with varying position and nature of alkyl substituents. Here, a change of the position of the substituent can diminish the donor ability of the pyrazolyl unit to the value of the pyridinyl unit. This study allows new insights into the donor competition in transition metal bis(pyrazolyl)methane complexes.

Experimental Section

All reactions were carried out under a dry nitrogen atmosphere in a glove box. The solvents were degassed and dried following a standard procedure [24]. IR measurements were done with an FT/IR-460 Plus instrument from Jasco using an ATR unit. HR-ESI-MS experiments were performed on a Thermo Finnigan LTQ FT Ultra Fourier Transform Ion cyclotron resonance mass spectrometer with an IonMax ion source (4 kV, 250 °C, MeCN). A sheathgas flow of 25 units and a sweepgas flow of 5 units were applied. Magnetic susceptibility data were collected using a MPMSXL-5 SQUID magnetometer under an applied field of 0.5 T over the temperature range 10 to 400 K in the settle mode. The samples were placed in gelatin capsules held within a plastic straw under argon protective atmosphere. The data were corrected for the diamagnetic contributions of the ligands by using tabulated Pascal's constants.

All DFT calculations were conducted using GAUSSIAN 09 (revision B.01) [25] and the implemented NBO3, as well as the stand-alone NBO6 [26] for all second-order perturbation theory calculations.

[Fe{HC(Pz)$_2$(Py)}$_2$][CF$_3$CO$_2$]$_2$, ***1[CF$_3$CO$_2$]$_2$***

Iron(II) trifluoroacetate (77.3 mg) was dissolved in 2 mL CH_2Cl_2 and was added to a solution of HC(Pz)$_2$(Py) (56.3 mg) in 2 mL CH_2Cl_2. The mixture was stored at room temperature. After 24 h the complex crystallised as orange blocks (90 %). – IR (cm^{-1}): ν = 3135 vw, 2977 vw, 2870 w, 1782 vw, 1672 m (ν(C=O)), 1515 vw, 1478 w, 1436 w, 1407 m, 1368 vw, 1325 vw, 1280 m, 1249 w, 1190 s (ν(C–F)), 1139 vs (ν(C–F)), 1092 m, 1058 m, 1029 m, 993 m, 907 m, 875 m, 842 m, 799 m, 764 m, 731 m, 716 m, 691 m, 657 m. – HRMS ((+)-ESI, THF, m/z (%)): calcd.: 619.1229, found: 619.1229 (7) [M–(CF$_3$CO$_2$)]$^+$, calcd.: 394.0214, found: 394.0213 (100) [M–(CF$_3$CO$_2$)–HC(Pz)$_2$(Py)]$^+$, calcd.: 253.0689, found: 253.0687 (12) [M–2(CF$_3$CO$_2$)]$^{2+}$.

[Fe{HC(3-iPrPz)(5-iPrPz)(Py)}$_2$][CF$_3$SO$_3$]$_2$, ***2[CF$_3$SO$_3$]$_2$***

Iron(II) triflate (88.5 mg) was dissolved in 2 mL THF and added to a solution of HC(3-*i*PrPz)$_2$(Py) (77.3 mg) in 2 mL THF. The mixture was stored at room temperature. After 48 h the complex crystallised as yellow needles (30 %). – IR (cm^{-1}): ν = 3116 vw, 2980 w, 2934 vw, 2873 w, 1606 w, 1525 w, 1482 w, 1451 vw, 1434 w, 1420 m, 1385 w, 1338 vw, 1277 s, 1249 vs (ν(C–F)), 1224 m, 1156 s (ν(C–F)), 1076 w, 1049 w, 1028 vs (ν(S=O)), 951 vw, 878 w, 849 vw, 835 w, 789 m, 764 m (ν(S–O)), 742 m, 729 w, 676 w. – HRMS ((+)-ESI, THF, m/z (%)): calcd.: 823.1277, found: 823.1780 (32) [M–(CF$_3$SO$_3$)]$^+$, calcd.: 514.0823 , found: 514.0823 (100) [M–(CF$_3$SO$_3$)–HC(3-*i*PrPz)(5-*i*PrPz)(Py)]$^+$, calcd.: 337.1628, found: 337.1627 (29) [M–2(CF$_3$SO$_3$)]$^{2+}$.

[Fe{HC(3-iPrPz)(5-iPrPz)(Py)}$_2$][FeBr$_4$]Br·2C$_4$H$_8$O, ***2[FeBr$_4$]Br***

Iron(II) bromide (53.9 mg) and HC(3-*i*PrPz)$_2$(Py) (77.3 mg) were dissolved in 10 mL THF, and both solutions were combined. The mixture was stored at room temperature. After 48 h the complex crystallised in low yields as orange rods (10 %). – IR (cm^{-1}): ν = 3083 w, 2966 m, 2929 w, 2869 w, 2796 vw, 1674 w, 1604 w, 1590 w, 1573 w, 1555 vw, 1525 m, 1476 m, 1446 m, 1419 m, 1386 m, 1364 m, 1343 w, 1324 w, 1290 m, 1238 m, 1213 m, 1155 w, 1108 w, 1072 m, 1048 m, 1019 m, 995 w, 961 w, 946 w, 904 w, 876 m, 849 m, 838 m, 824 m, 803 m, 781 s, 756 vs, 742 s, 728 m, 692 w, 677 m, 658 m, 637 m, 625 m, 616 m. – HRMS ((+)-ESI, THF, m/z (%)): calcd.: 755.2419, found: 755.2419 (1) [Fe+2(HC(3-*i*PrPz)(5-*i*PrPz)(Py))+1^{48}Br]$^+$, calcd.: 753.2440 , found: 753.2442 (1) [Fe+2(HC(3-*i*PrPz)(5-*i*PrPz)(Py))+1^{46}Br]$^+$, calcd.: 337.1628, found: 337.1627 (100) [Fe+2(HC(3-*i*PrPz)(5-*i*PrPz)(Py))]$^{2+}$.

Crystal structure determinations

The crystal data were collected with a Bruker D8 Venture with Bruker-AXS SMART [25] APEX CCD, using Mo K$_\alpha$ radiation (λ = 0.71073 Å) and a graphite monochromator. Data reduction and absorption correction were performed with SAINT and SADABS [27]. The structure was solved by Direct Methods and conventional Fourier syntheses. All non-hydrogen atoms were refined anisotropically with full-matrix least-squares based on F^2 (XPREP [28]; SHELXL [29]). Hydrogen atoms were derived from difference Fourier maps and placed at idealised positions, riding on their parent C atoms, with isotropic displacement parameters U_{iso}(H) = 1.2U_{eq}(C) and 1.5U_{eq}(C methyl). All methyl groups were allowed to rotate but not to tip. In **1[CF$_3$CO$_2$]$_2$** it was not possible to model the disordered solvent molecules (CH_2Cl_2) in an adequate manner, and the data set was treated with the SQUEEZE routine as implemented in PLATON [30, 31].

CCDC 1016618 (**1[CF$_3$CO$_2$]$_2$**), 1016619 (**2[CF$_3$SO$_3$]$_2$**) and 1016620 (**2[FeBr$_4$]Br**) contain the supplementary crystallographic data for this paper. These data can be obtained free of charge from The Cambridge Crystallographic Data Centre *via* www.ccdc.cam.ac.uk/data_request/cif.

Acknowledgement

The research leading to these results has partially been supported by the European Commission's Seventh Framework Programme (FP7/2007-2013) under grant agreement no. 312579 (ER-flow). We thank the Deutsche Forschungsgemeinschaft (SFB749-B10) for financial support. Generous grants of computing time at the Paderborn Center for Parallel Computing PC^2 are gratefully acknowledged.

[1] N. Kitajima, Y. Moro-oka, *Chem. Rev.* **1994**, *94*, 737 – 757.
[2] K. Fujisawa, A. Tateda, Y. Miyashita, K.-I. Okamoto, F. Paulat, V. K. K. Praneeth, A. Merkle, N. Lehnert, *J. Am. Chem. Soc.* **2008**, *130*, 1205 – 1213.
[3] N. Lehnert, U. Cornelissen, F. Neese, T. Ono, Y. Noguchi, K.-I. Okamoto, K. Fujisawa, *Inorg. Chem.* **2007**, *46*, 3916 – 3933.
[4] N. Burzlaff, *Angew. Chem. Int. Ed.* **2009**, *48*, 5580 – 5582.
[5] H. Kopf, B. Holzberger, C. Pietraszuk, E. Hübner, N. Burzlaff, *Organometallics* **2008**, *27*, 5894 – 5905.
[6] E. Hübner, G. Türkoglu, M. Wolf, U. Zenneck, N. Burzlaff, *Eur. J. Inorg. Chem.* **2008**, 1226 – 1235.
[7] A. Beck, B. Weibert, N. Burzlaff, *Eur. J. Inorg. Chem.* **2001**, 521 – 527.

[8] T. Godau, A. L. Müller, S. M. Bleifuss, T. Roth, S. Hoffmann, F. W. Heinemann, N. Burzlaff, *Dalton Trans.* **2011**, *40*, 6547 – 6554.
[9] A. Hoffmann, C. Citek, S. Binder, A. Goos, M. Rübhausen, O. Troeppner, I. Ivanović-Burmazović, E. C. Wasinger, T. D. P. Stack, S. Herres-Pawlis, *Angew. Chem. Int. Ed.* **2013**, *52*, 5398 – 5401.
[10] A. Hoffmann, S. Herres-Pawlis, *Chem. Commun.* **2014**, *50*, 403 – 405.
[11] H. Beyer, W. Francke, W. Walter, *Lehrbuch der Organischen Chemie*, S. Hirzel Verlag, Stuttgart, **2004**.
[12] D. L. Reger, T. C. Grattan, *Synthesis* **2003**, *3*, 350 – 356.
[13] A. Hoffmann, S. Herrres-Pawlis, *Z. Anorg. Allg. Chem.* **2013**, *639*, 1426 – 1432.
[14] A. Hoffmann, U. Flörke, S. Herres-Pawlis, *Eur. J. Inorg. Chem.* **2014**, 2296 – 2306.
[15] P. K. Byers, A. J. Canty, R. T. Honeyman, *J. Organomet. Chem.* **1990**, *385*, 417 – 427.
[16] C. Wilfer, A. Hoffmann, S. Herres-Pawlis, manuscript in preparation.
[17] F. Blasberg, J. Bats, M. Bolte, H. Lerner, M. Wagner, *Inorg. Chem.* **2010**, *49*, 7435 – 7445.
[18] A. Hoffmann, U. Flörke, S. Herres-Pawlis, *Inorg. Chem. Commun.* **2012**, *22*, 154 – 157.
[19] P. Gütlich, Y. Garcia, H. A. Goodwin, *Chem. Soc. Rev.* **2000**, *29*, 419 – 427.
[20] W. Bauer, W. Scherer, S. Altmannshofer, B. Weber, *Eur. J. Inorg. Chem.* **2011**, 2803 – 2818.
[21] T. M. Pfaffeneder, S. Thallmair, W. Bauer, B. Weber, *New. J. Chem.* **2011**, *35*, 691 – 700.
[22] W. Bauer, C. Lochenie, B. Weber, *Dalton Trans.* **2014**, *43*, 1990 – 1999.
[23] S. Schlamp, P. Thoma, B. Weber, *Eur. J. Inorg. Chem.* **2012**, 2759 – 2768.
[24] D. B. G. Williams, M. Lawton, *J. Org. Chem.* **2010**, *75*, 8351 – 8354.
[25] M. J. Frisch, G. W. Trucks, H. B. Schlegel, G. E. Scuseria, M. A. Robb, J. R. Cheeseman, G. Scalmani, V. Barone, B. Mennucci, G. A. Petersson, H. Nakatsuji, M. Caricato, X. Li, H. P. Hratchian, A. F. Izmaylov, J. Bloino, G. Zheng, J. L. Sonnenberg, M. Hada, M. Ehara, K. Toyota, R. Fukuda, J. Hasegawa, M. Ishida, T. Nakajima, Y. Honda, O. Kitao, H. Nakai, T. Vreven, J. A. Montgomery, Jr., J. E. Peralta, F. Ogliaro, M. Bearpark, J. J. Heyd, E. Brothers, K. N. Kudin, V. N. Staroverov, T. Keith, R. Kobayashi, J. Normand, K. Raghavachari, A. Rendell, J. C. Burant, S. S. Iyengar, J. Tomasi, M. Cossi, N. Rega, J. M. Millam, M. Klene, J. E. Knox, J. B. Cross, V. Bakken, C. Adamo, J. Jaramillo, R. Gomperts, R. E. Stratmann, O. Yazyev, A. J. Austin, R. Cammi, C. Pomelli, J. W. Ochterski, R. L. Martin, K. Morokuma, V. G. Zakrzewski, G. A. Voth, P. Salvador, J. J. Dannenberg, S. Dapprich, A. D. Daniels, O. Farkas, J. B. Foresman, J. V. Ortiz, J. Cioslowski, D. J. Fox, GAUSSIAN 09 (revision B.01), Gaussian, Inc., Wallingford CT (USA) **2010**.
[26] E. D. Glendening, C. R. Landis, F. Weinhold, *J. Comp. Chem.* **2013**, *34*, 1429 – 1437.
[27] SMART (version 5.62), SAINT (version 6.02), SHELXTL (version 6.10) and SADABS (version 2.03), Bruker Analytical X-ray Instruments Inc., Madison, Wisconsin (USA) **2002**.
[28] XPREP, Bruker Analytical X-ray Instruments Inc., Madison, Wisconsin (USA) **2007**.
[29] G. M. Sheldrick, *Acta Crystallogr.* **2008**, *A64*, 112 – 122.
[30] A. L. Spek, PLATON, A Multipurpose Crystallographic Tool, Utrecht University, Utrecht (The Netherlands) **2008**.
[31] A. L. Spek, *Acta Crystallogr.* **2009**, *D65*, 148 – 155.